On the mechanical behaviour of dry cohesionless soils by DEM simulations

Dorival M. Pedroso, Sergio Galindo-Torres & David J. Williams
The University of Queensland, Brisbane, Australia

This paper presents a study on the macroscopic mechanical characteristics of granular assemblies (dry cohesionless soils) with three dimensional complex shaped (non-spherical) particles. The study is conducted using the discrete element method (DEM) with the so-called sphero-polyhedra particles and simulations of mechanical true triaxial tests for a range of Lode angles. Focus is given to the strength characteristics. The observed mathematical failure envelopes are investigated in the Haigh-Westergaard stress space. It is verified that the DEM simulations with complex particles are more stable than with spheres, either considering virtual rolling resistance or not. It is also verified that the discrete element method with non-spherical particles produces results qualitatively similar to experimental data on the Toyoura sand. The simulations reproduce quite well the strength of assemblies of granular media such as higher strength during compression than during extension. Finally, it is observed that the Matsuoka-Nakai failure envelope averages very well the simulated data and that the macroscopic friction angle can be considered constant for the range of mean pressures investigated, both for spheres and sphero-polyhedra.

1 INTRODUCTION

The mechanical properties of assemblies of natural grains, such as dry cohesionless soils, are determined primarily by particle size, surface texture, size distribution, and shape of grains. Another important property is the structure of the packing, such as cubic, pyramidal, or tetrahedral. The packing also affects the porosity and density. These properties are basically of physical nature and have great influence on the macroscopic behaviour such as strength of the assembly. In this paper, attention is given to the capabilities of a numerical model in predicting the strength of assemblies of non-spherical particles. Dense packings of polyhedron-shaped particles with rounded corners, the so-called sphero-polyhedra, are considered. Numerical simulations are carried out using the discrete element method (DEM).

Previous works on the two dimensional properties of assemblies of polygonal shaped particles are available (Alonso-Marroquín and Herrmann 2002; Alonso-Marroquín and Herrmann 2005; Galindo-Torres et al. 2010) and some works consider also three-dimensional particles of non-spherical shapes (Galindo-Torres et al. 2009; Wang et al. 2010; Galindo-Torres and Pedroso 2010), although not all discuss the mechanical behaviour and strength properties of cubic assemblies, in particular the shape of the failure envelopes in the Haigh-Westergaard space.

Experimentally, the macroscopic mechanical behaviour of granular assemblies can be investigated using triaxial cells, as is customary in Soil Mechanics. Cylindrical cells are usually employed; however, with these cells, only a two dimensional (axis-symmetric) stress field can be generated. On the other hand, by using cubical, or *true* triaxial cells, the investigation of the three principal components of stress and strains can be carried out; hence, allowing the observation of the influence of the Lode angle on the octahedral plane.

Usually, macroscopic phenomenological criteria such as the Mohr-Coulomb are fitted to the observed data collected through triaxial tests. These criteria are then used to predict the strength of the granular assembly. Loading tests with shearing and stress paths in which the mean stress is kept constant are convenient for the investigation of the pattern of the peak stresses on the octahedral plane. Therefore, the shape of the failure envelope on this plane can be assessed as well.

Matsuoka and Nakai (Matsuoka and Nakai 1974) presented a failure criterion that predicts the same strength for compression and extension as the Mohr-Coulomb criterion; however its predictions for intermediate stresses (influence of the second stress eigenvalue) exhibit higher strength than the Mohr-Coulomb criterion – this is often indicated by tests

on soils and other granular media. Moreover, the Matsuoka-Nakai criterion has a smooth envelope on the octahedral plane – a great convenience for numerical models – and is product of intensive research on the mechanical properties of soils, leading to the concept of the *Spatially Mobilized Plane* (SMP) (Matsuoka and Nakai 1977; Nakai 1980; Matsuoka and Nakai 1982; Nakai and Matsuoka 1983; Matsuoka and Nakai 1985). The spatially mobilized plane forms a convenient and rational framework for the definition of continuum models for granular matter.

Other criteria that define failure envelopes with similar shape to that of the Matsuoka-Nakai criterion were proposed in the literature (Argyris et al. 1974; von Wolffersdorff 1996). However, the lack of convexity of the failure envelopes of some of these criterion may cause problems to numerical simulations (Pedroso et al. 2008). The main algebraic difference is that while the Matsuoka-Nakai failure criterion is defined directly as a function of the characteristic invariants I_k of the stress tensor, the other criteria are defined by functions of the ratio between the deviatoric (q) and mean (p) stress invariants with respect to the Lode angle θ; the so-called $M = q/p := M(\theta)$ methods.

A goal of this research is to observe the shape of the failure envelopes that best fit the results of DEM simulations; therefore, virtual true triaxial tests are carried out. In the following, the methods are briefly explained but further details can be found in (Galindo-Torres et al. 2009; Galindo-Torres and Pedroso 2010; Galindo-Torres et al. 2011). One key step for the true triaxial test is the packing generation, which is carefully explained here. Afterwards, the modelling of the virtual true triaxial apparatus is discussed and a brief review of some common failure criteria in Soil Mechanics is presented. Results with spheres considering (and not) the so-called rolling resistance are presented as well.

2   METHODS

Cubic ensembles of particles are mechanically loaded and the deformations are measured. The kinematics and dynamics of each single particle are computationally represented and the macroscopic behaviour is observed. The problem is solved using the discrete element method (DEM) as originally presented by Cundall and Strack (Cundall and Strack 1979) except that some modifications are adopted in order to account for multi-contact and particles of complex (quasi-general) shape, including non-convex particles (Galindo-Torres et al. 2009; Galindo-Torres and Pedroso 2010; Galindo-Torres et al. 2011).

A main innovation of the method employed here is the use of a technique for the smoothing of the particles in which all edges have actually the shape
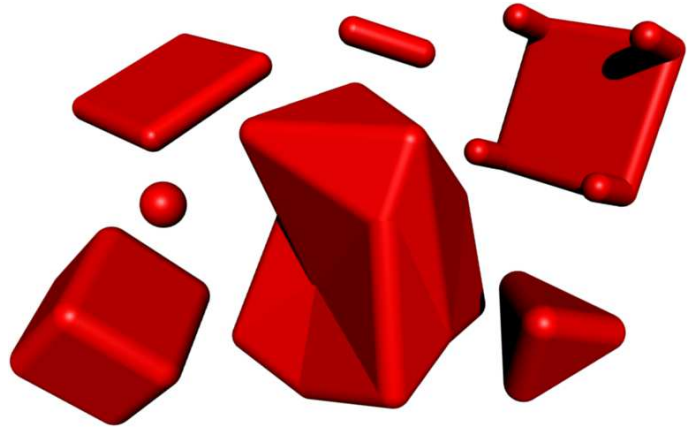

Figure 1: Some sphero-polyhedral particles, including convex and non-convex particles. All edges are of capsule-shape due to the smoothing with a given sphero-radius. Particles can be made of just one vertex, or one edge, or one face

of pharmaceutical pills or capsules (see examples in Fig. 1). This technique names the particles as sphero-polyhedra (Alonso-Marroquín 2008; Galindo-Torres et al. 2009; Galindo-Torres and Pedroso 2010; Galindo-Torres et al. 2011). Basically, all edges are swept by spheres, turning them into capsules, where the radius R of the sweeping sphere defines the sphero-radius of the particle. The faces will then have a thickness equal to $2R$ and smooth corners. The geometry of each particle is defined by a set of vertices, edges, and faces. Different shaped particles can be present in the same simulation; thus a complicate mix of particles of quasi-general shape can be simulated at the same time (Fig. 1). This technique largely simplifies the numerical method, since now the contact forces have a unique definition, contrary to schemes employing polygons or polyhedra.

The mass properties of the sphero-polyhedra particles are a little more difficult to be calculated than the mass properties of conventional polyhedra. The main reason is the rounding (smoothing) of the edges by applying the sweeping method. Therefore, closed form equations are unavailable, except, perhaps, for simple geometries, such as a rounded cube or a tetrahedron. To solve this problem, a numerical integration with the Monte-Carlo method is employed. The integration finds the volume (hence the mass), the tensor of inertia, and the centre of mass of the particles by Monte-Carlo approximations. These procedures also work for non-convex particles as the ones illustrated in Fig. 1.

2.1   Particle generation

Dense cubic packings of irregular particles are generated using the method discussed in (Galindo-Torres and Pedroso 2010). Due to its importance for the true triaxial simulations in this paper, the method is further explained here. The method is named *Voronoi-erosion*
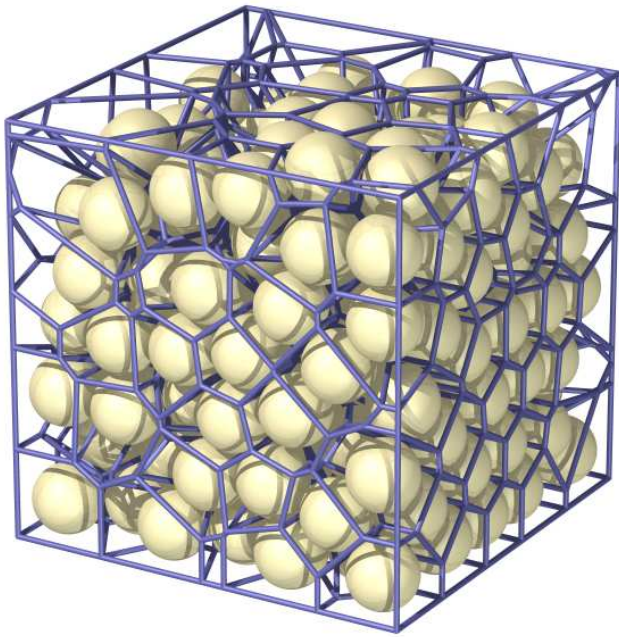
Figure 2: Voronoi tessellation generated by Voro++ (extracted from its online documentation). The yellow spheres are shown in order to help the visualization of the 3D lattice only and are not used as particles here. Particles are created by the erosion algorithm described in the text, considering the "Voronoi-cells" defined by the blue edges.

since it is based on the Voronoi tessellation (Voronoi 1907) and requires an algorithm for the erosion of the initial assembly of particles. The erosion is required mainly because the particles need to be converted into sphero-polyhedra, i.e. have all edges smoothed, and no overlapping should be present at the beginning of the simulations, otherwise the system would not be at equilibrium.

A three-dimensional grid is first generated with the dimensions of the cubic sample, then random points are sampled in the interior of each grid cell. The number and position of the points will control the final particle size and distribution. With these points, another library, named *Voro++* (Rycroft 2009), is called in order to generate the Voronoi tessellation. One example of the output of Voro++ is shown in Fig. 2, extracted from its user manual (Rycroft 2009).

The Voronoi tessellation partitions the domain into cells as illustrated in Fig. 2. In this figure, the yellow spheres are shown to help the visualisation of the 3D volume only; they are not used as DEM particles in this research. Afterwards, with the 3D Voronoi tessellation (the blue edges in Fig. 2 defining the *Voronoi-cells*), particles are created by eroding the cells by an amount equal to the sphero-radii of the sphero-polyhedra. Basically, the faces and edges of a Voronoi-cell are displaced to the interior of the cell and all intersections are computed. A control for the

displacements must be applied, because if the displacements are too large, the solution may not exist and the cell may become degenerated. Therefore, the sphero-radii of the particles must be limited and their values are generally found by *trial-and-error*.

With this technique, the packing is ready for the true triaxial simulation, since the algorithm guarantees that no overlaps exist, i.e. the particles are already in perfect contact one with each other but not overlapping. Clearly, this technique can only create dense packings. Another method to generate the packing would be to run a preliminary DEM simulation with the application of gravity, in order to move the grains until a stable condition is found. Nonetheless, this method would create a geo-static situation where contact forces do exist; this is not the isotropic situation desired for the investigation in this research, especially at the first stage of the true triaxial testing – zero gravity situation.

By controlling the position and number of points randomly distributed inside the grid, the size and shape of the Voronoi particles can be indirectly controlled. However, in all analyses presented in this paper, the number was chosen in such a way that the assembly is reasonably isotropic with particles not too elongated or with small angles. This can be done by distributing equal, but random, spaced points. In addition, because of this construction, the size of the particles is approximately uniform. Further details are found in (Galindo-Torres et al. 2009; Galindo-Torres and Pedroso 2010).

Fig. 3 illustrates a cubic packing of 1000 spheropolyhedra created by the *Voronoi-erosion* technique and which is adopted as the experimental specimen for the numerical simulations of true triaxial tests.

3 TRUE TRIAXIAL TEST

The shear properties of granular assemblies can be obtained with samples subjected to either compression or extension stress paths. These tests allow for the investigation of the relationship between deviatoric stresses and mean stresses at failure, and hence the macroscopic friction properties. Shearing tests with stress paths in which the mean stress is kept constant allow for the investigation of the pattern of the ultimate stress points on the octahedral plane. Therefore, the shape of the failure envelope on this plane can be investigated as well. The true triaxial is a convenient apparatus to obtain these information.

The true triaxial apparatus is composed by a system of six rigid plates forming a parallelepiped. Because the DEM code employed in this work can handle complex (quasi-general) shaped particles, the loading plates of the apparatus can also be defined as DEM particles. This is very convenient since no change to the code is necessary in order to implement the
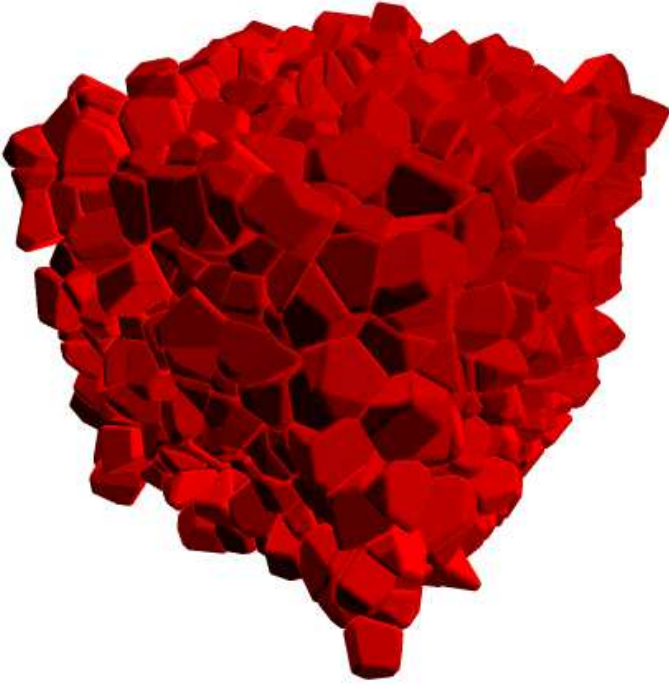
Figure 3: Cubic packing with 1000 quasi-general (sphero-polyhedra) particles used in the true triaxial tests, generated by means of the *Voronoi-erosion* technique.
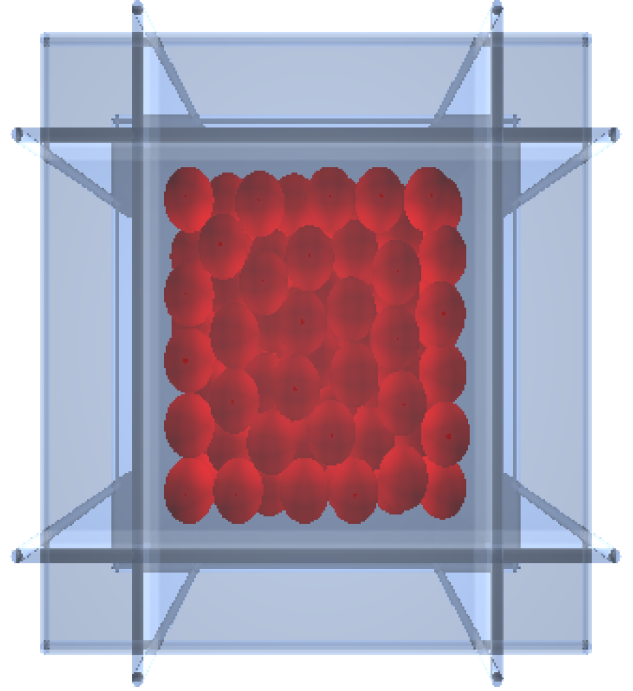

Figure 4: Cubic ensemble of spheres representing a sample for the true triaxial test. There are 1000 particles randomly generated. The same packing is used for simulations with and without rolling resistance. The loading plates of the apparatus can freely cross each other. There is no friction between the plates and the particles.

contact between the loading plates and the granular material representing the sample. The friction coefficient between the plates and the particles can easily be controlled – here, the friction coefficient is set to zero simulating lubricated walls. In addition, the interaction between the plates one with respect to each other is switched off; therefore, the plates can easily cross each other in order to confine the particles (see Fig. 4). Clearly, problems such as the interaction between plates do not exist in the virtual apparatus.

Forces are applied to the plates of the virtual apparatus according to a pre-defined stress path. To calculate the stresses, the cross-sectional areas for each direction are updated as the plates move. Stresses are defined as negative during compression (Classical Mechanics' convention). Principal strain components are calculated by the change on the distance between opposite plates divided by their initial distance. The following Continuum Mechanics' quantities are calculated:

$$p_{cam} = -\frac{\sigma_1 + \sigma_2 + \sigma_3}{3} \tag{1}$$

$$q_{cam} = \frac{\sqrt{(\sigma_1 - \sigma_2)^2 + (\sigma_2 - \sigma_3)^2 + (\sigma_3 - \sigma_1)^2}}{\sqrt{2}} \tag{2}$$

$$\varepsilon_v = \varepsilon_1 + \varepsilon_2 + \varepsilon_3 \tag{3}$$

$$\varepsilon_d = \frac{\sqrt{2}}{3}\sqrt{(\varepsilon_1 - \varepsilon_2)^2 + (\varepsilon_2 - \varepsilon_3)^2 + (\varepsilon_3 - \varepsilon_1)^2} \tag{4}$$

Therein, σ_i are the principal stress components and ε_i are the principal strain components, p_{cam} is the negative of the Cambridge mean stress invariant (Schofield

and Wroth 1968), q_{cam} is the Cambridge deviatoric stress invariant, ε_v is the volumetric strain, and ε_d is the deviatoric strain.

To verify the strength properties of cubic assemblies of granular media subject to the combination of three stress components, the stress paths illustrated in Fig. 5 can be applied. These allow the construction of the failure envelopes in the Haigh-Westergaard space. Each path is described as follows:

- (1) Initial confinement of the specimen by means of isotropic stresses;

- (2a) Conventional (cylindrical) compression tests with constant lateral stresses and increasing vertical stress;

- (2b) Conventional (cylindrical) extension tests with constant vertical stress and increasing lateral stresses;

- (3) p-constant tests with a combination of stresses such that a pre-defined constant Lode angle (θ) can be reproduced on the octahedral plane (see Fig. 6). These paths vary from extension ($\theta = -30°$) to compression ($\theta = +30°$).

The Lode angle is illustrated in Fig. 6 and is defined

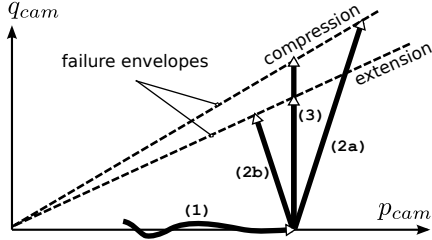Figure 5: Applied stress paths.

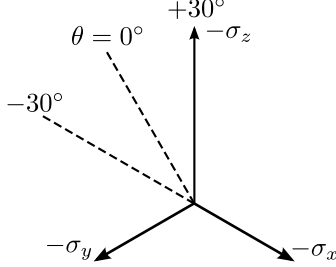Figure 6: Octahedral plane and definition of Lode angle θ.

according to the following expression:

$$\theta = \frac{1}{3} \operatorname{asin} \left(\frac{-27 s_1 s_2 s_3}{2 q_{cam}^3} \right) \qquad (5)$$

where s_i are the principal deviatoric stress components, calculated by means of: $s_i = \sigma_i + p_{cam}$.

4 FAILURE CRITERIA

Stress-based failure criteria can be defined by observing either the peak or the residual stresses attained in mechanical tests, such as triaxial tests. For instance, the ultimate stresses measured in triaxial tests with increasing deviatoric stresses can be used for this definition. Results from triaxial tests can be used to define failure criteria regarding either the macroscopic friction angle at compression ($\theta = +30°$) or the friction angle at extension ($\theta = -30°$). Only one these two angles is necessary for a mathematical model. In this paper, the results of friction angles at compression ϕ_{comp} are thus considered. After obtaining this single material parameter, the following criteria are fitted to the simulated data: Mohr-Coulomb, Matsuoka-Nakai, and Lade-Duncan (Lade and Duncan 1973).

The Mohr-Coulomb failure criterion predicts a linear relationship between q_{cam} and p_{cam} for the stress states at failure and can be mathematically expressed according to (disregarding cohesion):

$$\frac{\sigma_1^* - \sigma_3^*}{\sigma_1^* + \sigma_3^*} = \sin \phi_{comp} \qquad (6)$$

Therein, σ_i^* are the sorted (increasing) principal stress values. With this expression, the strength at extension will be smaller than for compression. Therefore, the shape of the Mohr-Coulomb failure envelope is of a deformed hexagon when viewed in the octahedral plane.

The Matsuoka-Nakai (Matsuoka and Nakai 1974) failure criterion predicts the same strength as the Mohr-Coulomb failure criterion for both compression and extension. For plane strain or when the Lode angle is in the range $-30° < \theta < +30°$, the Matsuoka-Nakai failure criterion predicts higher strength than the Mohr-Coulomb criterion. The Matsuoka-Nakai failure criterion is directly defined based on the three characteristic invariants I_i of the stress tensor according to

$$\frac{I_1 I_2}{I_3} = 9 + 8 \tan^2 \phi_{comp} \qquad (7)$$

Another failure criterion similar to the Matsuoka-Nakai failure criterion is the Lade-Duncan (Lade and Duncan 1973). This criterion predicts higher strength at extension than that predicted by the Matsuoka-Nakai or Mohr-Coulomb failure criteria. The Lade-Duncan criterion is given by

$$\frac{I_1^3}{I_3} = \frac{(3 - \sin \phi_{comp})^3}{(1 + \sin \phi_{comp})(1 - \sin \phi_{comp})^2} \qquad (8)$$

5 RESULTS

To observe the strength properties of cubic assemblies of granular media with the DEM, virtual true triaxial tests are carried out. The applied stress path is the one numbered (3) in Fig. 5, which is enforced after an initial isotropic compression is applied (path (1) in Fig. 5).

When using spherical particles, in order to account for the effect of eventual non-spherical shapes that are typically observed in natural grains, for instance in soils, the rolling resistance technique can be employed as a convenient alternative (Iwashita and Oda 1998). However, some artificial parameters have to be introduced. For the sake of comparison, simulations with spheres and rolling resistance are carried out and the scheme presented in (Luding 2008) for modelling the rolling resistance is adopted in this study.

Simulations of true triaxial tests are carried out with assemblies of spheres (Fig. 4) and sphero polyhedra (Fig. 3). The packings are randomly generated as described earlier in this paper. With spheres, simulations are carried out with and without rolling resistance. Each simulation is repeated with a different number of particles in order to also investigate the influence of the number of particles. The microscopic constants adopted in all analyses are organized in Table 1. In the following, p_{cte} means constant p_{cam}.

5.1 Linear model

Tests with spheres, spheres with rolling resistance, and sphero-polyhedra are carried out in order to verify whether the macroscopic strength of a cubic packing of grains can be represented by a linear model or not.

Table 1: Microscopic constants for the DEM analyses.

Constant	Description
$K_n = 10000.0$	Contact normal stiffness
$K_t = 5000.0$	Contact tangential stiffness
$\mu = 0.4$	Microscopic friction coefficient
$g_n = 8.0$	Normal viscous coefficient
$g_t = 0.0$	Tangential viscous coefficient
$\beta = 0.12$	Rolling resistance stiffness coefficient *(only for spheres with rolling resistance)*
$\eta = 1.0$	Plastic moment coefficient *(only for spheres with rolling resistance)*
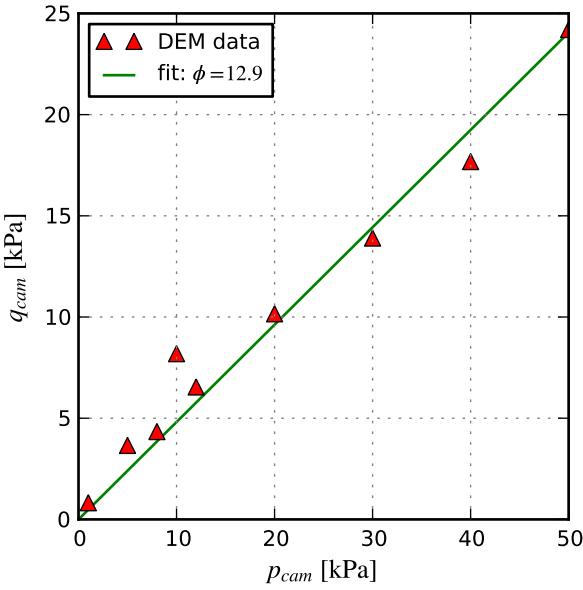
Figure 7: Tests with 1000 spheres under compression (path (3) with constant p_{cam}).

Figure 8: Tests with 10000 spheres under compression (path (3) with constant p_{cam}).

The linear model here applies to the relationship between deviatoric and mean stresses. The compression ($\theta = +30°$) path with p-constant is employed for such task.

Results with 1000 spheres and 10000 spheres are given in Fig. 7 and Fig. 8, respectively. It is observed that the results with 1000 spheres are more scattered (noisy) than those obtained with 10000 spheres. For the latter, the boundary conditions have less influence and the representative volume (RVE) is better defined because of the higher number of particles.

To illustrate the difference on material response due to the number of particles, the stress-strain curves for each one of the packings with 1000 spheres and 10000 spheres are given in Fig. 9 and Fig. 10, respectively, where it can be seen that the increase on the number of particles makes the simulation more stable with qualitatively better representation when compared with real materials; Toyoura sand for instance.

The stability situation and the quality of representation are improved by adding rolling resistance to
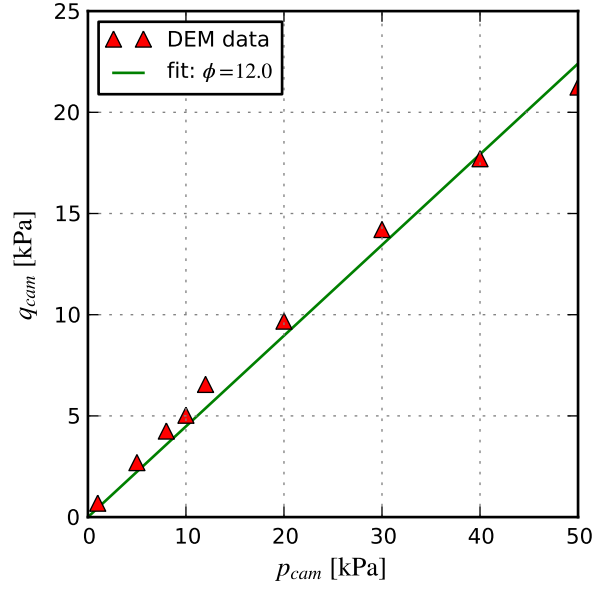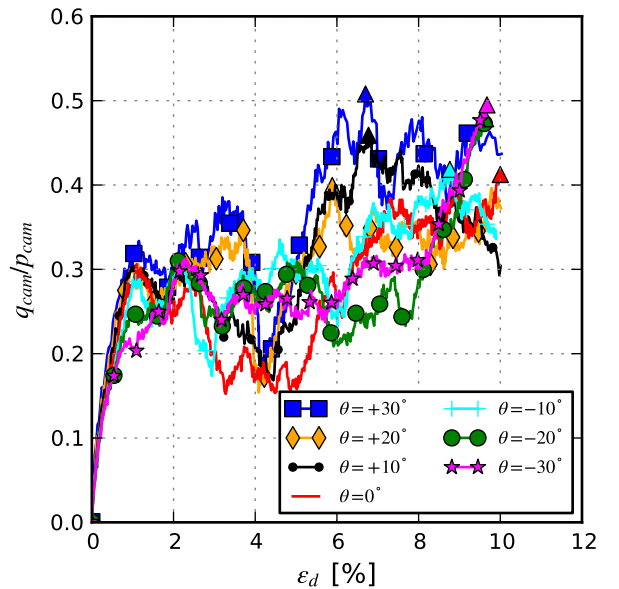

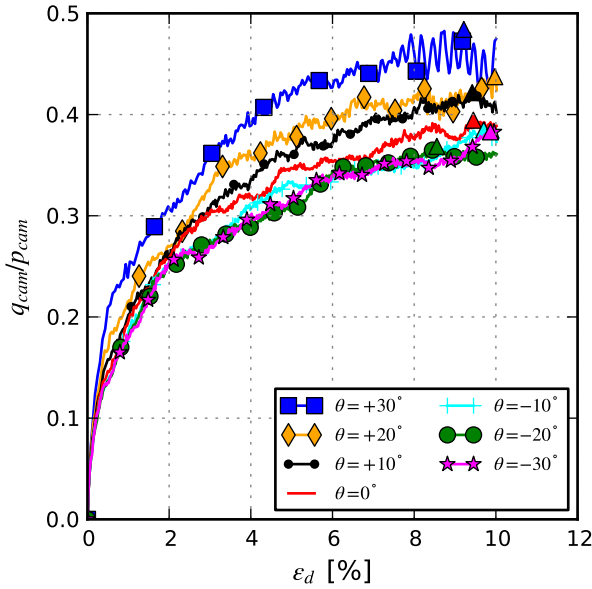Figure 9: Stress-strain behaviour of a sample with 1000 spheres ($p_{cte} = 20\,\text{kPa}$).

Figure 10: Stress-strain behaviour of a sample with 10000 spheres ($p_{cte} = 20\,\text{kPa}$).

the assembly of spheres. This makes sense as long as the DEM has to reproduce Nature materials such as sands. The linear fitting in this case is illustrated in Fig. 11 and Fig. 12 for 1000 spheres and 10000 spheres, respectively. The results with 1000 particles are again more scattered than with 10000 particles.

Even though the results in Fig. 12 weakly suggest a nonlinear fitting, a linear model is adopted, since the selected points representing the peak stresses are not necessarily the most robust indication of failure stresses. It is important to note that these may vary somewhat from simulation to simulation and depend on the boundary conditions, REV size, and stress
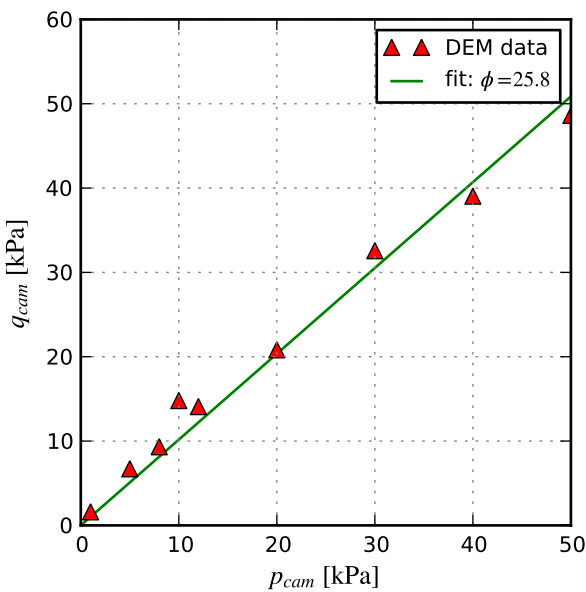
Figure 11: Tests with 1000 spheres with rolling resistance under compression (path (3) with constant p_{cam}).
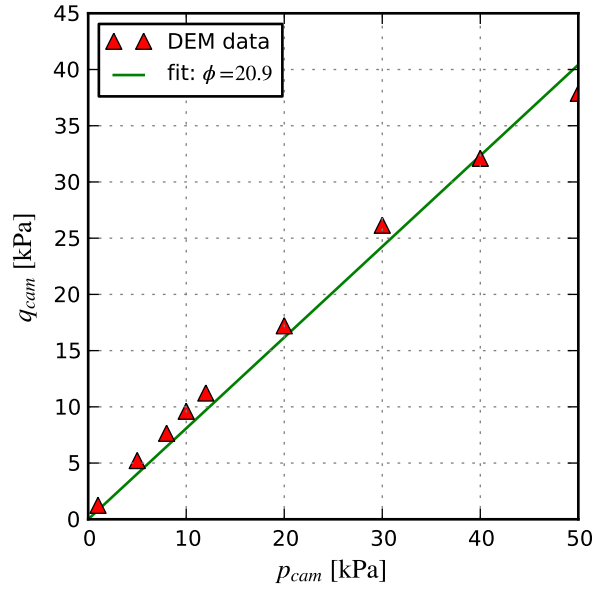
Figure 12: Tests with 10000 spheres with rolling resistance under compression (path (3) with constant p_{cam}).

path. Therefore, it is reasonable to adopt a linear fitting.

To illustrate the difficulty on selecting the points representing the failure states, stress-strain curves are plotted as in Figs. 13 and 14 (see also Figs. 9 and 10) for assemblies with 1000 particles and 10000 particles (spheres with rolling resistance), respectively. In these figures, the selected points are indicated by upward triangles (the same is done for all other stress-strain curves). With 10000 particles, there is less noise and the predicted curves are more similar to the ones obtained with real sand, as shown in a next section, i.e. the 10000 particles cube is a better REV.

Simulations of true triaxial tests are also carried out with assemblies of complex shaped particles (sphero-polyhedra). Different number of particles, from 1000 to 10000 are considered. It is observed that the stress-strain response does not change radically for these numbers of particles (see Fig. 15). This is due to the already high number of contacts in a sphero-polyhedra packing, therefore, well reproducing a dense granular packing. In Fig. 15, the macroscopic strength properties (ultimate stresses ratio) of the packing with complex particles are similar for each number of particles. For instance, the ultimate stress ratio at failure is about $q_{cam}/p_{cam} = 1.2$. Because of this similarity, only the tests with 1000 particles are further discussed in the following text.

The deviatoric-mean stresses relationship for the specimen of 1000 sphero-polyhedra (assembly illustrated in Fig. 3) is given in Fig. 16, for compression stress paths with constant mean pressure. It is observed that the data can be very well fitted by a straight line (linear model), contrary to the simulation
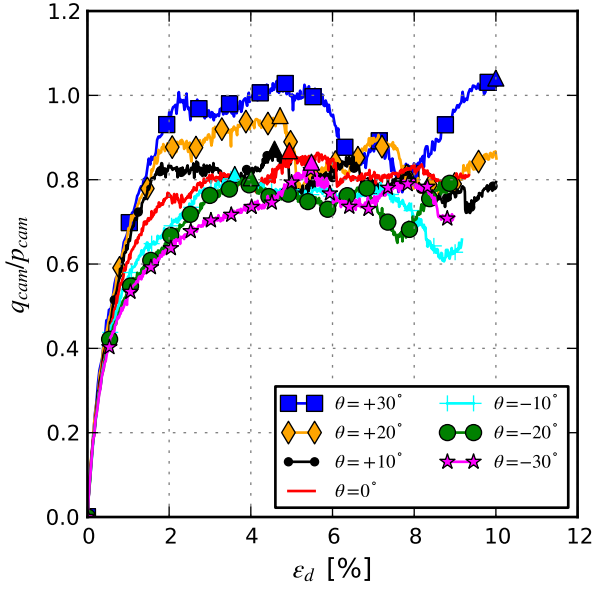
Figure 13: Stress-strain behaviour of a sample with 1000 spheres with rolling resistance ($p_{cte} = 20$ kPa).
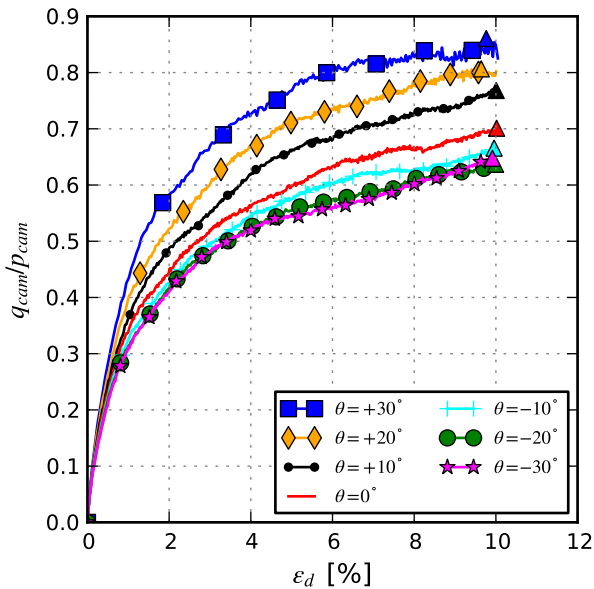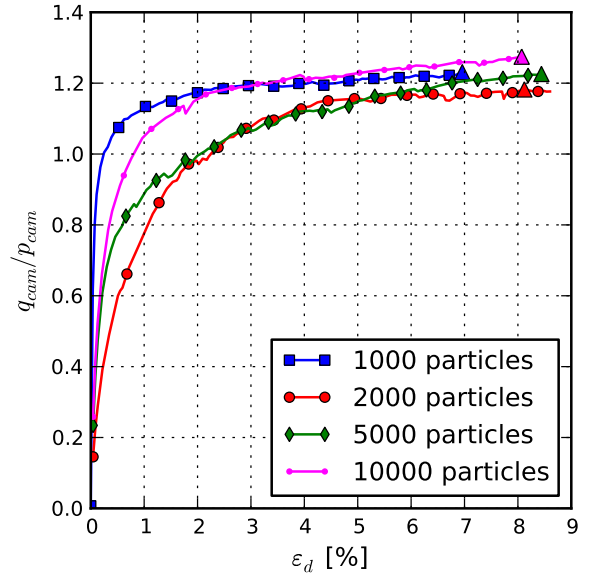

Figure 15: Stress-strain behaviour of samples of complex (sphero-polyhedra) particles ($p_{cte} = 5$ kPa).

with spheres with rolling resistance or not.

The stress-strain curves obtained with the 1000 sphero-polyhedra packing are also more smooth than that obtained with 1000 spheres with rolling resistance or not. This is mainly due to the higher number of contacts (vertices, edges, faces) and the interlocking provided by the complex shapes. The curves obtained with 1000 sphero-polyhedra can hence be compared with those obtained with 10000 spheres. Later, it is shown that the sphero-polyhedra packing qualitatively represents very well the Toyoura sand.

The stress-strain behaviour in this case is illustrated in Fig. 17 for a constant mean pressure of 20 kPa. The reason for a less chaotic behaviour of the sphero-polyhedra is related to the dissipation of the kinetic
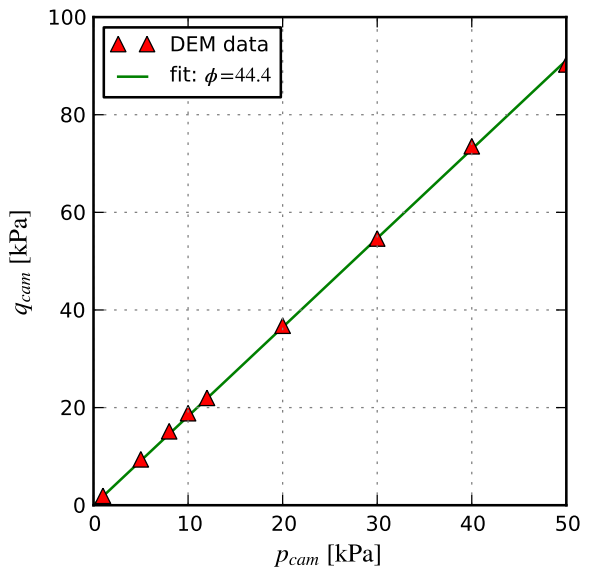

Figure 14: Stress-strain behaviour of a sample with 10000 spheres with rolling resistance ($p_{cte} = 20$ kPa).

Figure 16: Tests with 1000 sphero-polyhedra particles under compression (path (3) with constant p_{cam}).
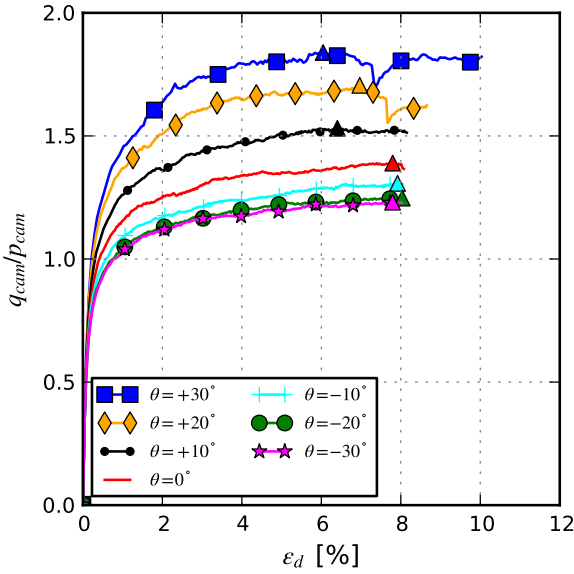
Figure 17: Stress-strain behaviour of a sample with 1000 sphero-polyhedra ($p_{cte} = 20\,\text{kPa}$).

energy. The noise observed with spheres is indeed of chaotic nature and its effect is mitigated by constraining particles movement (as with rolling resistance). When spheres are free to roll, the kinetic energy of the system is not as quickly dissipated as in the other constrained cases, hence producing a noisy response. On the other hand, the angularity of the sphero-polyhedra, and eventual multi-contact (non-convex particles), will produce a strong constraint for the particles movement in addition to a larger number of collisions for the same number of particles. This higher frequency of inelastic collisions will then reduce the kinetic energy and the noise.

5.2 Octahedral plane

The data obtained with DEM simulations of true triaxial tests are now plotted in the Haigh-Westergaard 3D space of principal stresses. In particular, a view along the hydrostatic axis is considered, with focus on the so-called octahedral plane. This allows the investigation of an appropriated macroscopic failure envelope for isotropic materials. Although the failure envelope is a 3D surface in the Haigh-Westergaard stress space, only its cross-section on the octahedral plane is drawn, for a fixed p_{cam} value.

For the mathematical definition of a particular failure criteria with linear deviatoric-mean stress relationship (e.g. Mohr-Coulomb, Matsuoka-Nakai, Lade-Duncan), a constant macroscopic friction angle must be defined beforehand. Either the angle at compression or extension can be employed for such task. Here ϕ_{comp} at compression is considered.

For spheres, as shown in Figs. 7, 8, 11, and 12, a constant friction angle may not fit all sets of data for all range of mean stresses. For the case of $p_{cam} = 20\,\text{kPa}$, the fitting seems to be fairly accurate. This
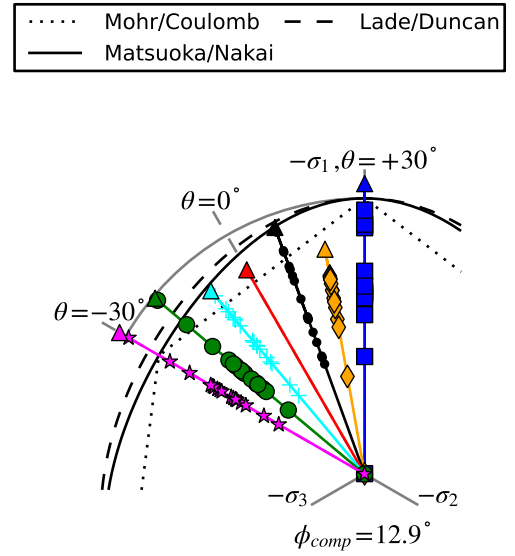

Figure 18: Octahedral view of data obtained with 1000 spheres ($p_{cte} = 20\,\text{kPa}$).

case is then selected to illustrate the DEM results on the octahedral plane, including the shape of some failure criteria. These results are given in Figs. 18, 19, 20, 21.

For the packing with 1000 sphero-polyhedra, the constant friction angle fits quite well all data obtained with different values of p_{cam}. The results for $p_{cam} = 20\,\text{kPa}$ are given in Fig. 22.

For spheres, spheres with rolling resistance, and sphero-polyhedra, it is observed that most data lie in between the Mohr-Coulomb criterion (lower bound) and the Lade-Duncan criterion (upper bound), with
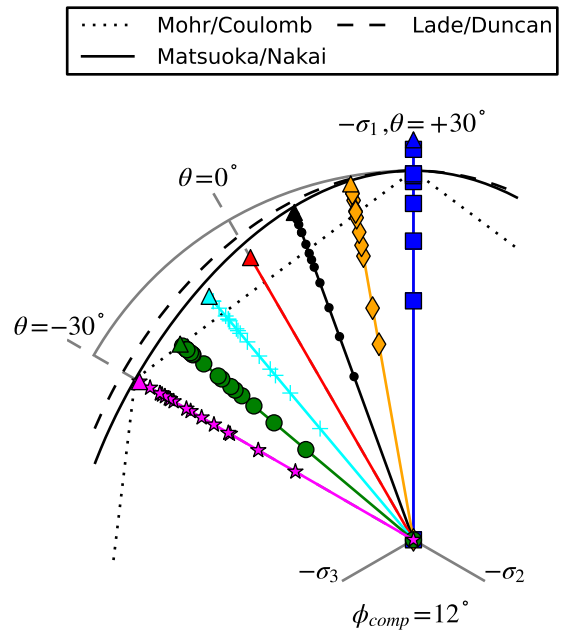

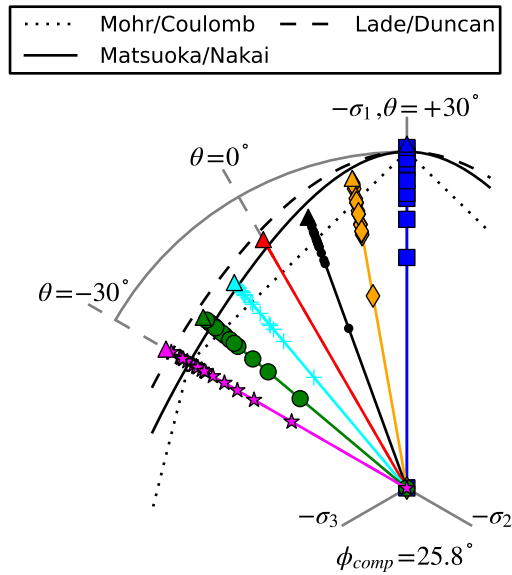Figure 19: Octahedral view of data obtained with 10000 spheres ($p_{cte} = 20\,\text{kPa}$).

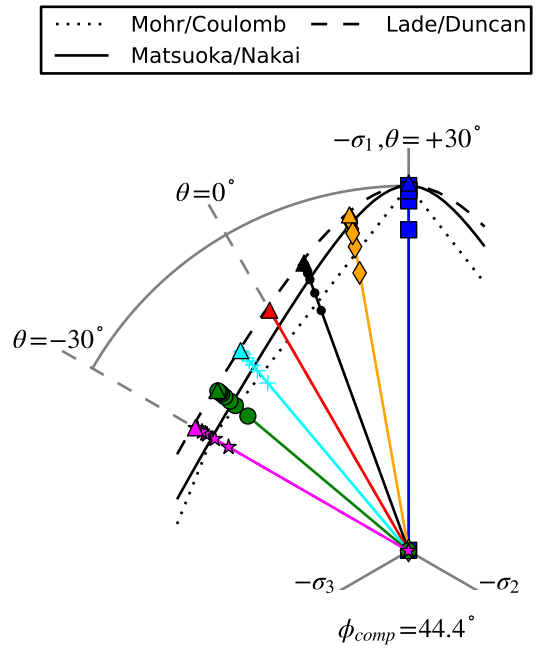Figure 20: Octahedral view of data obtained with 1000 spheres with rolling resistance ($p_{cte} = 20\,\text{kPa}$).

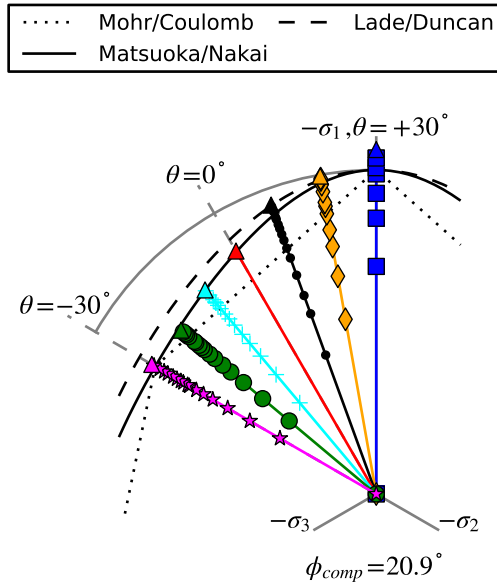Figure 22: Octahedral view of data obtained with 1000 sphero-polyhedra ($p_{cte} = 20\,\text{kPa}$).
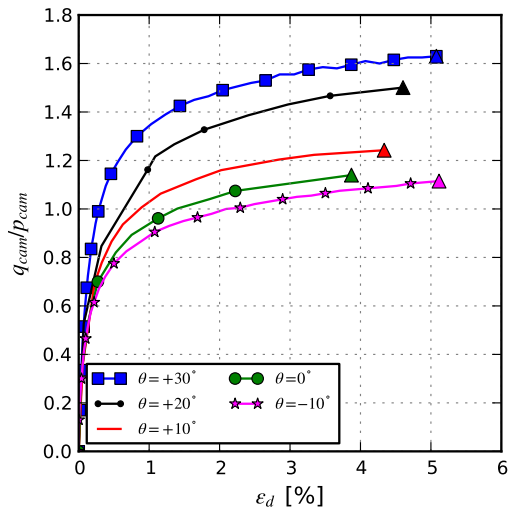
the Matsuoka-Nakai criterion being a good average. Regarding the sphero-polyhedra, it is interesting to note that the (isotropic) geometry of the (complex) particles does not affect much the shape of the failure envelope, apart from increasing the macroscopic friction angle, when compared with spheres.
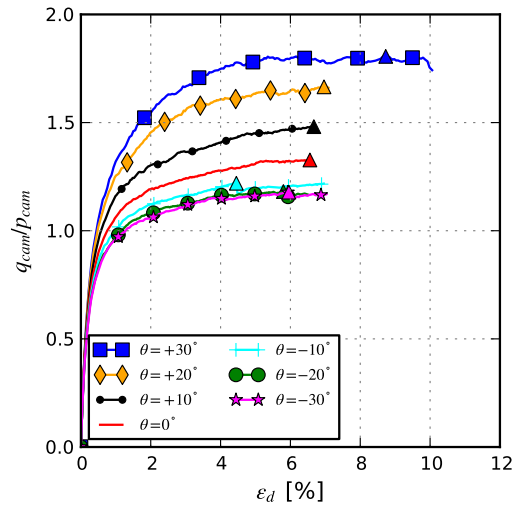
5.3 Qualitative observation

To asses the capabilities of the DEM on representing assemblies of complex shaped grains, real experimental data from true triaxial tests on the Toyoura sand of Japan (Nakai 1989), illustrated in Fig. 23(a,c,e), are qualitatively compared with the numerical results obtained with 1000 sphero-polyhedra, as given in Fig. 23(b,d,f). It can be observed that both the stress-strain behaviour (Fig. 23(a,b)) and dilatancy curves (Figs. 23(c,d)) of experimental data and simulations are quite similar, indicating that the 1000 particles packing of sphero-polyhedra is a reasonable representation of this particular sand, regarding the macroscopic mechanical behaviour.
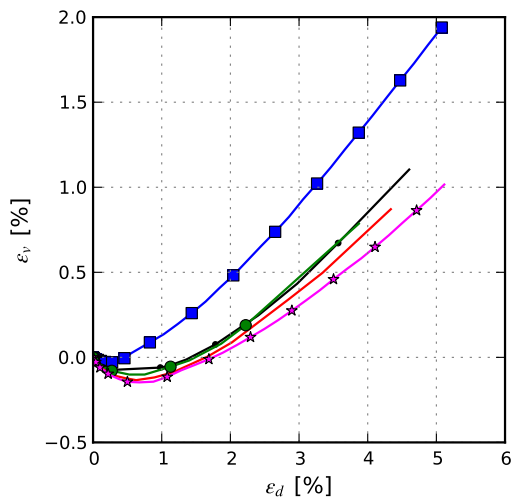
It can also be observed that the influence of the Lode angle is similar when comparing experiments with simulations. In particular, it can be seen that the strength at extension is smaller than at compression (Figs. 23(e,f)). This also illustrates the great importance of considering the stress path on the strength characteristics of granular materials. Finally, for both sets of data and predictions, ideal failure envelopes have similar shapes.

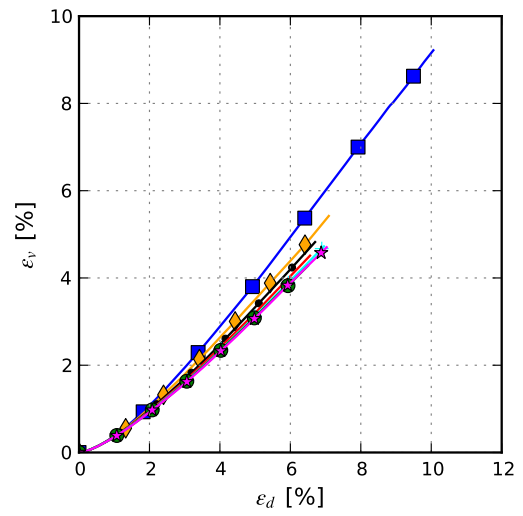Figure 21: Octahedral view of data obtained with 10000 spheres with rolling resistance ($p_{cte} = 20\,\text{kPa}$).
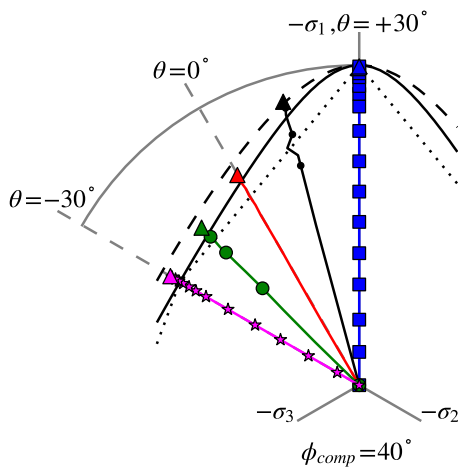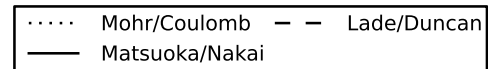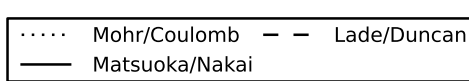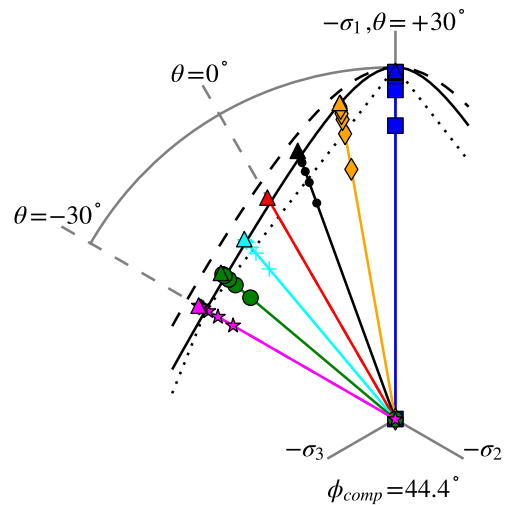
(a) Toyoura sand

(b) Sphero-polyhedra

(c) Toyoura sand

(d) Sphero-polyhedra

(e) Toyoura sand

(f) Sphero-polyhedra

Figure 23: Comparison of experimental data on Toyoura sand (left, $p_{cte} = 196\,\mathrm{kPa}$, data after Nakai, 1989) with DEM results with 1000 sphero-polyhedra (right, $p_{cte} = 50\,\mathrm{kPa}$).

6   CONCLUSIONS

A DEM code that considers grains of non-spherical (quasi-general) shapes is employed for simulations of cubic packings representing true triaxial tests. Attention is given to the strength properties of assemblies of granular media. The pattern of the failure data both on the octahedral and on the deviatoric-mean pressure planes are observed.

The generation of dense packings of complex particles is carried out employing a three-dimensional Voronoi tessellation, after which an erosion algorithm is applied in order to build sphero-polyhedral particles, i.e. smooth particles with rounded edges.

Non-physical corrections, such as the virtual rolling resistance technique, necessary for the simulations of Nature grains, such as sands or gravels, are completely avoided by the method employed in this research thanks to the consideration of particles of quasi-general (complex) shapes.

It is verified that the DEM simulations with sphero-polyhedra are more stable than with spheres, either with or without rolling resistance. This is mainly due to the interlocking of the grains that may cause more dissipation of energy, and, therefore, more damping, in addition to provide a higher frequency for contacts. Because the number of contacts in assemblies of sphero-polyhedra may be higher than in assemblies of spheres, the number of particles in packings of sphero-polyhedra may be smaller than in packings of spheres.

The instabilities of DEM simulations with spheres are a reported problem in the DEM literature related to simulations of natural grains and one of the solutions is precisely the adoption of rolling resistance. However, the rolling resistance introduces virtual (non-physical) parameters. The instabilities are mainly due to the rolling of grains that do not depend on the friction angle. Controlling the rolling prevents this chaotic behaviour. The non-spherical shape of sphero-polyhedra is a much more natural solution, allowing a sound physical representation of natural materials.

It is also verified that, for all particles studied here, spherical or sphero-polyhedral, the relationship between deviatoric and mean stresses at failure (for peak stresses) is best fitted with a straight line. This implies that the best phenomenological model for this material is a linear model with constant macroscopic friction coefficient. In addition, it is verified that the stress values at failure, when plotted on the octahedral plane, usually lie between the Mohr-Coulomb and the Lade-Duncan envelopes with the Matsuoka-Nakai model being a good average.

The numerical results qualitatively agree with a set of experimental data on Toyoura sand. Therefore, the DEM, especially with particles more similar to real Nature grains (non-spherical), can describe quite well the macroscopic properties of granular assemblies, including higher strength at compression than at extension and an intermediate strength from compression to extension.

REFERENCES

Alonso-Marroquín, F. (2008). Spheropolygons: A new method to simulate conservative and dissipative interactions between 2d complex-shaped rigid bodies. *EPL (Europhysics Letters) 83*(1), 14001.

Alonso-Marroquín, F. and H. J. Herrmann (2002, Aug). Calculation of the incremental stress-strain relation of a polygonal packing. *Phys. Rev. E 66*(2), 021301.

Alonso-Marroquín, F. and H. J. Herrmann (2005). The incremental response of soils. an investigation using a discrete-element model. *Journal of Engineering Mathematics 52*, 11–34.

Argyris, J. H., G. Faust, J. Szimmat, E. P. Warnke, and K. J. Willam (1974). Recent developments in the finite element analysis of prestressed concrete reactor vessels. *Nuclear Engineering and Design 28*, 42–75.

Cundall, P. A. and O. D. L. Strack (1979). A discrete numerical model for granular assemblies. *Géotechnique 29*(1), 47–65.

Galindo-Torres, S. A., F. Marroquín, Y. Wang, D. M. Pedroso, and J. Castaño (2009). Molecular dynamics simulation of complex particles in three dimensions and the study of friction due to nonconvexity. *Physical Review E 79*(6).

Galindo-Torres, S. A., J. D. Muñoz, and F. Alonso-Marroquín (2010). Minkowski-voronoi diagrams as a method to generate random packings of spheropolygons for the simulation of soils. *Phys. Rev. E 82*(5), 056713.

Galindo-Torres, S. A. and D. M. Pedroso (2010). Molecular dynamics simulations of complex-shaped particles using voronoi-based spheropolyhedra. *Phys. Rev. E 81*(6), 061303.

Galindo-Torres, S. A., D. M. Pedroso, D. J. Williams, and L. Li (2011). Breaking processes in three-dimensional bonded granular materials with general shapes. *Computer Physics Communications 183*(2), 266–277.

Iwashita, K. and M. Oda (1998). Rolling resistance at contacts in the simulation of shear band development by DEM. *Journal of Engineering Mechanics ASCE 124*(3), 285–292.

Lade, P. V. and J. M. Duncan (1973). Cubical triaxial tests on cohesionless soil. *Journal*

of Soil Mechanics and Foundations Division (ASCE) 99(10), 793–812.

Luding, S. (2008). Cohesive, frictional powders: contact models for tension. *Granular Matter 10*(4), 235–246.

Matsuoka, H. and T. Nakai (1974). Stress-deformation and strength characteristics of soil under three different principal stresses. In *Proc. JSCE*, Number 232, pp. 59–70.

Matsuoka, H. and T. Nakai (1977). Stress strain relationship of soil based on the SMP. In *Proc. speciality session 9, 9th ICSMFE*, pp. 153–162.

Matsuoka, H. and T. Nakai (1982). A new failure criterion of soils in three-dimensional stresses. In *Conference on deformation and failure of granular materials - IUTAM*, Delft, USA, pp. 253–263.

Matsuoka, H. and T. Nakai (1985). Relationship among tresca, mises, mohr-coulomb and matsuoka-nakai failure criteria. *Soil and Foundations 25*(4), 123–128.

Nakai, T. (1980). *Deformation and strength characteristics of soils and its application to deformation analysis of ground*. Ph. D. thesis, Kyoto University. In japanese.

Nakai, T. (1989). An isotropic hardening elasto-plastic model for sand considering the stress path dependency in three-dimensional stresses. *Soils and Foundations 29*(1), 119–137.

Nakai, T. and H. Matsuoka (1983). Shear behaviors of sand and clay under three dimensional stress condition. *Soil and Foundations 23*(2), 26–41.

Pedroso, D. M., D. Sheng, and S. W. Sloan (2008). Stress update algorithm for elastoplastic models with nonconvex yield surfaces. *International Journal for Numerical Methods in Engineering 76*(13), 2029–2062.

Rycroft, C. H. (2009). Voro++: a three-dimensional voronoi cell library in c++. *To apper in 'Chaos'*.

Schofield, A. and P. Wroth (1968). *Critical State Soil Mechanics*. McGraw Hill.

von Wolffersdorff, P. (1996). A hypoplastic relation for granular materials with a predefined limit state surface. *Mechanics of Cohesive-Frictional Materials 1*, 251–271.

Voronoi, G. (1907). Nouvelles applications des paramètres continus à la theorie des formes quadratiques. *Journal für die Reine und Angewandte Mathematik 133*, 97–178.

Wang, J., H. Yu, P. Langston, and F. Fraige (2010). Particle shape effects in discrete element modelling of cohesive angular particles. *Granular Matter*, 1–12.